Dual Mode Interferometer for Measuring Dynamic Displacement of Specular and Diffuse Components

Michael North Morris, Tim Horner, Markar Naradikian, Joe Shiefman
4D Technology Corporation, 3280 E. Hemisphere Loop Suite 146, Tucson, AZ 85706
(520) 294-5600, (520) 294-5601 fax, michael.north-morris@4dtechnology.com

Abstract:

We present a dual mode interferometer system based on a single-frame phase acquisition sensor that is capable of measuring the dynamic displacement of both specular and diffuse components. The single frame acquisition allows the interferometer to freeze the motions of the test articles in both configurations and examine the dynamic nature of the surface figure under dynamic stress. The system has applications in the testing of dynamic optical components such as deformable mirrors as well as defect detection and structural stability of composite materials. This paper will provide an overview of the interferometer design, outline the different measurement configurations and present measurement results of dynamically excited test articles.

Keywords: Interferometer, Spatial Phase-Shifting, Dynamic, Vibration Insensitivity, ESPI, Speckle

1. Introduction

As dynamic Interferometry matures and more applications come to light, there is a greater demand for compact flexible interferometer systems that can be integrated into complex test setups and provide additional functionality. For instance, interferometers are commonly incorporated into large optic polishing and generating machines for in-situ measurements, often the same test set-up is used for measuring both the surface shape of a mirror and the stability of the back plane that holds the mirror. Also, many industries are interested in measuring surfaces that are moving at high velocities.

The interferometer presented here addresses some of these new requirements by providing a compact flexible design that enables dynamic measurements of both specular and diffuse surfaces with minimal changes between configurations. The dimensions of the interferometer are 175mm x 162mm x 83mm, allowing it to easily be placed in complex test setups. In addition, the dual mode operation allows one interferometer to take the place of what has traditionally been done by two different interferometers. Additionally, this interferometer captures all of the required phase-shifted interference patterns in one camera frame, which facilitates measurements of dynamic components in challenging environments.

Optical Inspection and Metrology for Non-Optics Industries, edited by Peisen S. Huang, Toru Yoshizawa, Kevin G. Harding, Proc. of SPIE Vol. 7432, 74320W · © 2009 SPIE · CCC code: 0277-786X/09/$18 · doi: 10.1117/12.827090

The following sections provide an overview of the interferometer design, outline the different measurement configurations and present measurement results of dynamically excited test articles.

2. Phase-Shifting Techniques

The heart of the system lies in a pixelated phase-mask where each pixel has a unique phase-shift.[1] By arranging the phase-steps in a repeating pattern, fabrication of the mask and processing of the data can be simplified. A small number of discrete steps can be arranged into a "unit cell" which is then repeated contiguously over the entire array. The unit cell can be thought of as a super-pixel; the phase across the unit cell is assumed to change very little. By providing at least three discrete phase-shifts in a unit cell, sufficient interferograms are produced to characterize a sample surface using conventional interferometric algorithms. Figure 1 illustrates a unit cell comprised of four discrete phase steps. Other combinations are possible; however, four phase steps provide optimal sampling. The example shows the phase-steps are in quadrature. For best resolution, a one-to-one correspondence is preferably used between the phase-mask and the detector pixels.

The overall system concept is also shown in Figure 1. and consists of a polarization interferometer that generates a reference wavefront R and a test wavefront T having orthogonal polarization states (which can be linear as well as circular) with respect to each other; a pixelated phase-mask that introduces an effective phase-delay between the reference and test wavefronts at each pixel and subsequently interferes the transmitted light; and a detector array that converts the optical intensity sensed at each pixel to an electrical charge. The pixelated phase-mask and the detector array may be located in substantially the same image plane, or positioned in conjugate image planes.

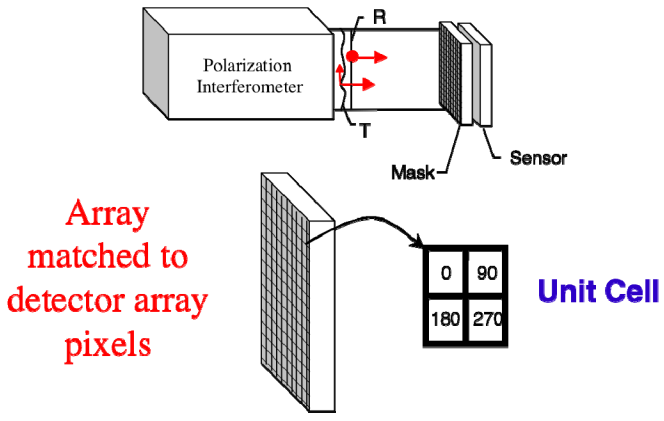

Figure 1. Basic concept for the pixelated phase-mask dynamic interferometer.

In principle, a phase-mask shown in Figure 1 could be constructed using an etched birefringent plate, however, such a device is difficult to manufacture accurately. An alternative approach is to use an array of micropolarizers. Kothiyal and Delisle[2] showed that the intensity of two beams having orthogonal circular polarization (i.e., right-hand circular and left-hand circular) that are interfered by a polarizer is given by

$$I(x,y)=\frac{1}{2}\left(I_r+I_s+2\sqrt{I_r I_s}\cos\left(\Delta\phi(x,y)+2\alpha_p\right)\right) \tag{2.1}$$

where α_p is the angle of the polarizer with respect to the x, y plane. The basic principle is illustrated in Figure 2. From this relation it can be seen that a polarizer oriented at zero degrees causes interference between the in-phase (i.e., 0°) components of the incident reference and test wavefronts R and T. A polarizer oriented at 45 degrees interferes the in-phase quadrature (i.e., 90°) component between the incident reference and test wavefronts R and T. A polarizer oriented at 90 degrees interferes the out-of-phase (i.e., 180°) component between the incident reference and object wavefronts R and T. Finally, a polarizer oriented at 135 degrees interferes the out-of-phase quadrature (i.e., 270°) component between the incident reference and test wavefronts R and T.

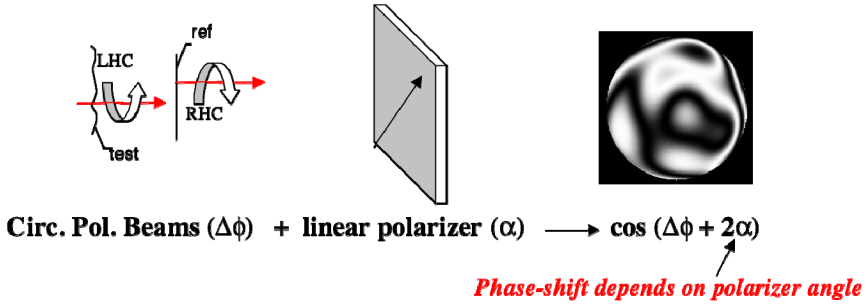

Figure 2. Basic principal of pixilated phase-shift inteferometer.

3. Data Processing

The effective phase-shift of each pixel of the polarization phase-mask can have any spatial distribution; however, it is highly desirable to have a regularly repeating pattern. A preferred embodiment for the polarization phase-mask is based on an arrangement wherein neighboring pixels are in quadrature or out-of-phase with respect to each other; that is, there is a ninety-degree or one hundred eighty degree relative phase shift between neighboring pixels.

Figure 1 illustrates one possible way of arranging the polarization phase-mask and detector pixels and for processing the measured data. The signal measured at each sensor pixel is given

by its transfer function, the phase-difference between the reference and test beams, and the amplitude of each beam. For example, one possible configuration is,

$$A(x,y)=\frac{1}{2}\left(I_r+I_s+2\sqrt{I_rI_s}\cos\left(\Delta\phi(x,y)\right)\right) \tag{3.1}$$

$$B(x,y)=\frac{1}{2}\left(I_r+I_s+2\sqrt{I_rI_s}\cos\left(\Delta\phi(x,y)+\frac{\pi}{2}\right)\right) \tag{3.2}$$

$$C(x,y)=\frac{1}{2}\left(I_r+I_s+2\sqrt{I_rI_s}\cos\left(\Delta\phi(x,y)+\pi\right)\right) \tag{3.3}$$

$$D(x,y)=\frac{1}{2}\left(I_r+I_s+2\sqrt{I_rI_s}\cos\left(\Delta\phi(x,y)+\frac{3\pi}{2}\right)\right) \tag{3.4}$$

wherein $I_r(x,y)$ and $I_s(x,y)$ are the intensities of the reference and test wavefronts R and T at each x, y coordinate in the image, respectively, and $\Delta\phi(x,y)$ is the optical path difference between the reference and test wavefronts.

Multiple interferograms can thus be synthesized by combining pixels with like transfer functions. To generate a continuous fringe map that opticians are accustomed to viewing for alignment, pixels with transfer functions can be combined into a single image or interferogram. For example all the pixels with transfer function A can be combined into a single image. The resulting interferogram can be displayed on a screen in real-time. The B, C, and D pixels can be similarly combined to produce corresponding interferograms. The resulting interferograms have a total number of pixels equal to (n x m)/N, where n and m are the numbers of pixels in the detector array in the x and y directions, respectively, and N is the number of different discrete phase-shift elements in the pixelated phase mask. In the above examples N is equal to four. The resulting four interferograms can be processed by a variety of algorithms that are well-known in the art for calculating phase difference and modulation index.[3] For example, a possible implementation for measuring phase difference is a simple four-bucket algorithm, e.g.,

$$\phi(x,y)=ATAN\left(\frac{\left(C(x,y)-A(x,y)\right)}{\left(D(x,y)-B(x,y)\right)}\right) \tag{3.5}$$

where the values A, B, C, and D are taken from adjacent neighboring pixels. Similarly, a modulation index map can be generated (similar to the phase-difference map) using the formula

$$\gamma(x,y)=\frac{2\sqrt{\left(A(x,y)-C(x,y)\right)^2+\left(D(x,y)-B(x,y)\right)^2}}{D(x,y)+B(x,y)+A(x,y)+C(x,y)} \tag{3.6}$$

An alternative method for calculating the phase difference at each spatial coordinate is to combine the measured signals of neighboring pixels in a fashion similar to a windowed convolution algorithm. This method provides an output phase-difference map having a total number of pixels equal to (n-W) times (m-V), where W and V are the sizes of the correlation window in the x and y directions, respectively. Thus, the resolution of the phasemap is close to the original array size, although the spatial frequency content has been somewhat filtered by the convolution process.

4. Measurement Modes

While the single frame acquisition provided by the pixilated phase mask is the key component that enables dynamic measurements, the geometry of the interferometer provides the flexibility required to easily switch between measuring specular and diffuse components. A fiber fed source module makes it possible to illuminate the test article on-axis from within the interferometer for specular surfaces or off-axis from a fiber launch for diffuse surfaces, an adjustable half-wave plate allows the relative irradiance of the test and reference beams impinging on the camera to be adjusted for best interference contrast, and an adjustable quarter waveplate near the entrance aperture of the interferometer facilitates generating and accepting a circularly polarized test beam when measuring specular surfaces and linear polarization when measuring diffuse surfaces.

Figure 3 shows both measurement configurations. For specular surfaces the bulk of the laser power is directed into a beam trap and a small portion is launched into a Twyman-Green interferometer via a polarization maintaining fiber where it is collimated. The collimated beam passes through an adjustable half-wave plate and is split into orthogonally polarized test and reference beams by a polarizing beam splitter. The relative power in the test and reference beams is continuously adjustable by rotating the half-wave plate. The reference beam passes through a quarter-wave plate oriented to produce circularly polarized light, reflects off the reference mirror and passes through the quarter-wave plate a second time. The linearly polarized light returning from the reference path reflects off the polarizing beam splitter and is directed onto the camera with the pixilated mask via a quarter waveplate that generates the required circularly polarized light. The test arm also has a quarter-wave plate that generates a circularly polarized test beam and rotates the linear polarization leaving the polarizing beam splitter 90 degrees. The difference is that the test beam is polarized horizontally and the reference beam is polarized vertically. As a result, after passing through the quarter-wave plate before the camera the test and reference beams are orthogonally circularly polarized. The test arm is shown with a diverging optic that is used to generate a spherical wavefront that closely matches the radius of curvature of the optic under test.

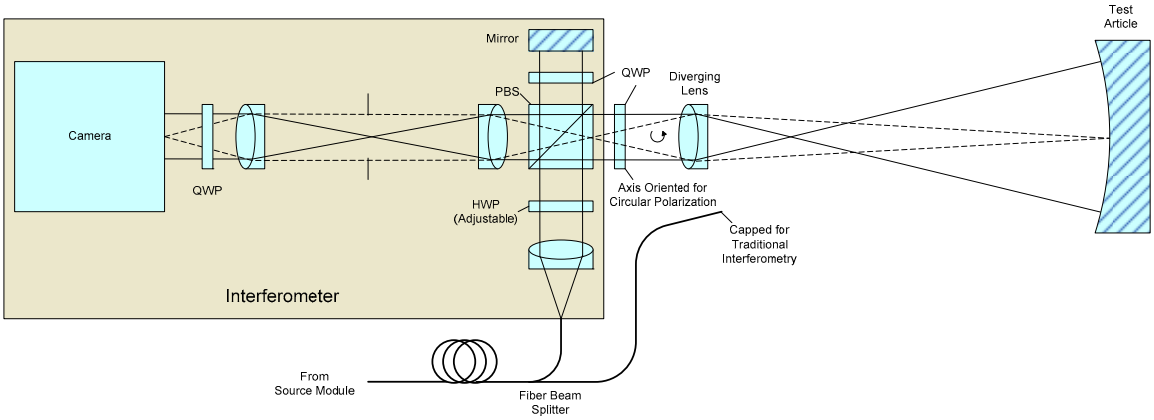

Figure 3a) Traditional Interferometry Configuration

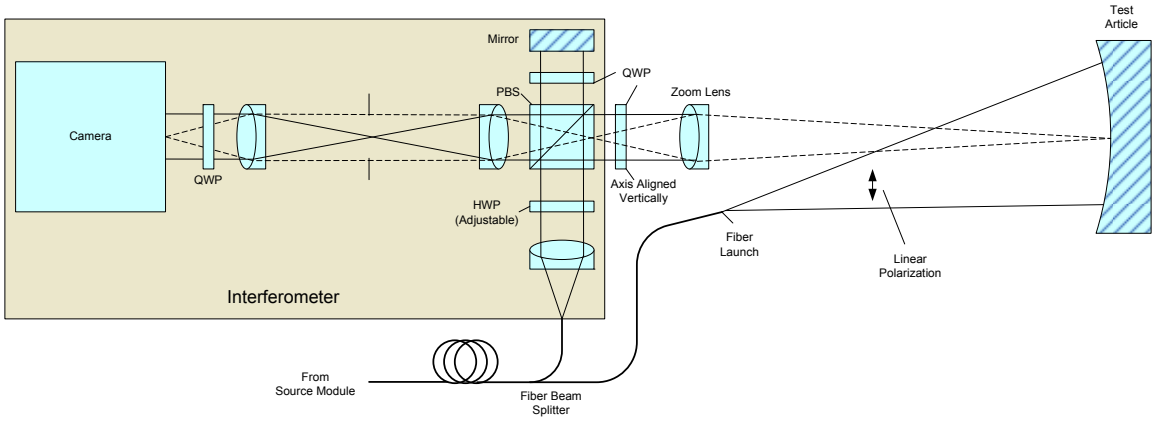

Figure 3b) Electronic Speckle Pattern Interferometry Configuration

When measuring a diffuse surface the configuration is changed slightly. The bulk of the light is used to illuminate the test article, the quarter-wave plate in the test arm is rotated such that its ordinary axis is aligned vertically effectively removing its impact on the test beam polarization and the diverging optic is replaced with an imaging lens. While the reference beam path is unchanged the test beam no longer emanates from within the interferometer. The small amount of light that is reflected by the polarizing beam splitter out of the interferometer no longer has its polarization rotated by the quarter-wave plate and if reflected back into the system is directed toward the fiber launch. The external illumination of the other hand has its polarization oriented horizontally by clocking the polarization maintaining fiber and passes through the polarizing beam splitter. The test article is imaged onto the camera via the imaging lens and an internal relay.

5. ESPI Review

Phase-shifted ESPI measurements are made by capturing two measurements one before and one after the surface is perturbed and subtracting the phase.[4,5,6] The phase subtraction can be

done directly in the phase domain; however, performing the subtraction in the interferogram domain before the arctangent is applied has the distinct advantage of facilitating the application of smoothing routines to reduce the sensitivity to random irradiance fluctuations. Although, the subtracting of two measurements significantly reduces the random irradiance pattern and enables the detection of correlation fringes, there is some speckle decorrelation between the frames resulting in fringes that are low contrast and noisy. Applying a smoothing function to the subtraction reduces the noise in the measurement and improves the contrast of the correlation fringes. The algorithm for performing the subtraction in the interferogram can be derived by applying the following trigonometric identity to the phase subtraction. [7]

$$Tan(a-b)=\frac{Tan(a)-Tan(b)}{1+Tan(a)\cdot Tan(b)} \tag{5.1}$$

The resulting algorithm is,

$$\Delta\phi_c = ArcTan\left(\frac{X(x,y)}{Y(x,y)}\right) \tag{5.2}$$

where

$$X(x,y)=[D_1(x,y)-B_1(x,y)]\cdot[A_2(x,y)-C_2(x,y)]-[A_1(x,y)-C_1(x,y)]\cdot[D_2(x,y)-B_2(x,y)]$$

$$Y(x,y)=[A_2(x,y)-C_2(x,y)]\cdot[A_1(x,y)-C_1(x,y)]+[D_1(x,y)-B_1(x,y)]\cdot[D_2(x,y)-B_2(x,y)]$$

A_1, B_1, C_1, D_1 are the phase-shifted interferograms for the baseline measurement and A_2, B_2, C_2, D_2 are the phase-shifted interferograms for the second measurement.

Noise in the measurement can be significantly reduced using a weighted spatial average over neighboring pixels. This can be accomplished by:

$$\Delta\phi_c(x,y) = ArcTan\left(\frac{\sum_{x,y\in\delta} X(x,y)}{\sum_{x,y\in\delta} Y(x,y)}\right), \tag{5.3}$$

where the sums are performed over a range of δ nearest neighbors. Because of the modulo 2π behavior of the arctangent function, the range is wrapped (ambiguous) beyond the wavelength of the source. Any number of well-known processes of spatial unwrapping can be used to remove the discontinuous steps and perform quantitative analysis of the interferograms.

6. Frequency Response

Dynamic interferometry implies the ability to make measurements in the presence of vibrations. The combination of spatial phase shifting and an extremely short integration time qualifies this interferometer as dynamic. The total integration time required to obtain all four phase-shifted frames can be as low as 30μs, over three orders of magnitude shorter than conventional interferometers.

The figure of merit for the dynamic performance of the interferometer is the fringe contrast reduction. The fringe contrast limited frequency response can be estimated by examining the fringe contrast reduction of a specular measurement in the presence of a single vibrational frequency, f. The expression for good fringe contrast is expressed mathematically as follows;

$$\frac{8\cdot\pi}{\lambda}\cdot A\cdot Sin\left(\pi\cdot\tau\cdot f\right)\leq 2\cdot\pi \qquad (6.1)$$

and

$$\tau << \frac{1}{f}$$

where A is the radial amplitude of the vibration, τ is the integration time for a single frame and λ is the wavelength of light. Integrating the fringe pattern over the integration time using the maximum velocity of the vibration and calculating the fringe contrast leads to the following expression for the fringe contrast.

$$V = Sinc\left(\frac{4\cdot A\cdot\pi^2\cdot\tau\cdot f}{\lambda}\right) \qquad (6.2)$$

Figure 4 shows the frequency response when the contrast reduction is limited to 50%. The sloping segment of the line is the region where the fringe contrast is reduced due to phase changes during the integration time as described by equation (3.2), the plateau below 5Hz, represents the fringe contrast reduction due to the high fringe density on the CCD and the cutoff at 266kHz represents a reduction in fringe contrast resulting from the integration time approaching the period of the vibration. The frequency response can be increased by using a pulsed laser or an acousto-optic light modulator to limit the integration times below the limit of the camera.

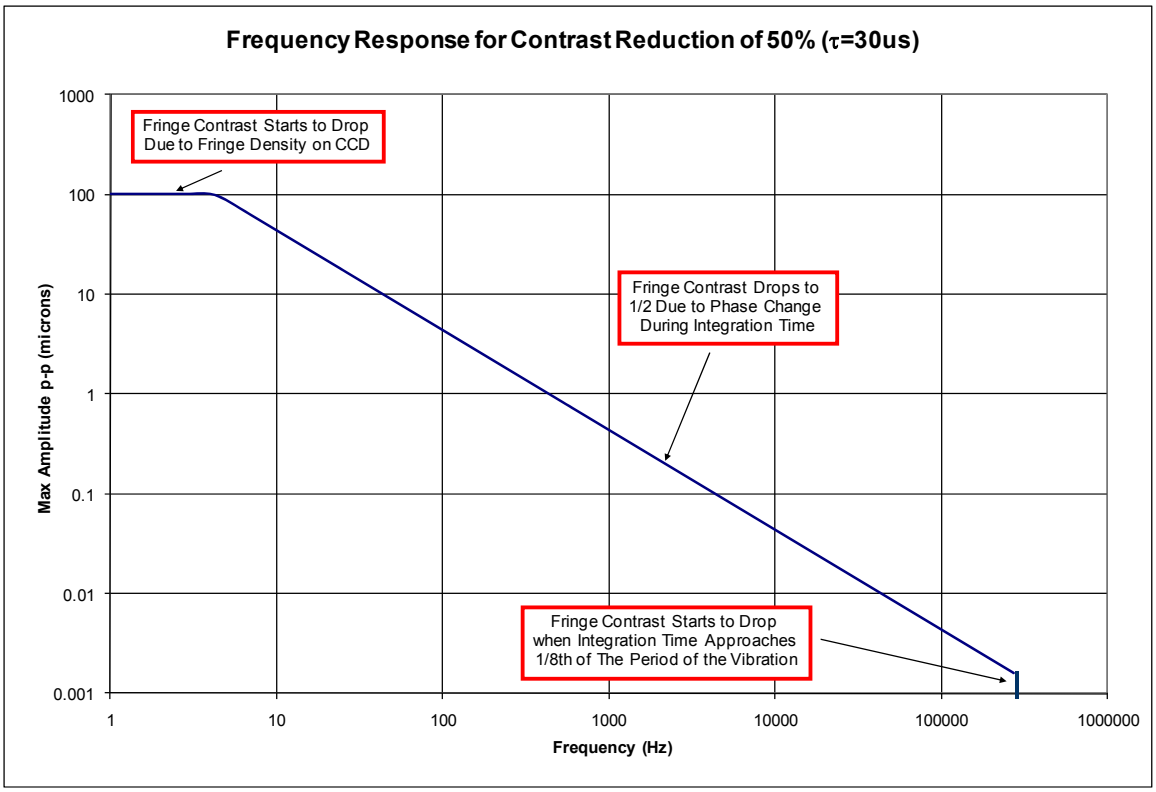

Figure 4: Frequency Response of Dynamic Interferometer

7. Dynamic Measurements

To demonstrate the dynamic capabilities of the interferometer two measurements of rapidly changing wavefronts were measured in ESPI mode. The measurement setup is shown in figure 5. The first dynamic measurement was of a metal diaphragm excited at its first resonant frequency. The change in the surface shape was measured asynchronously. Three measurements of the change in shape are shown in figure 6. The measured area had a diameter of approximately 1.25 inches, the resonant frequency was 4.1KHz and the peak-to-valley changes was approximately 0.2waves at 532nm. The area where the PZT leads connect to the diaphragm is noticeable as the asymmetric bump in the wavefront.

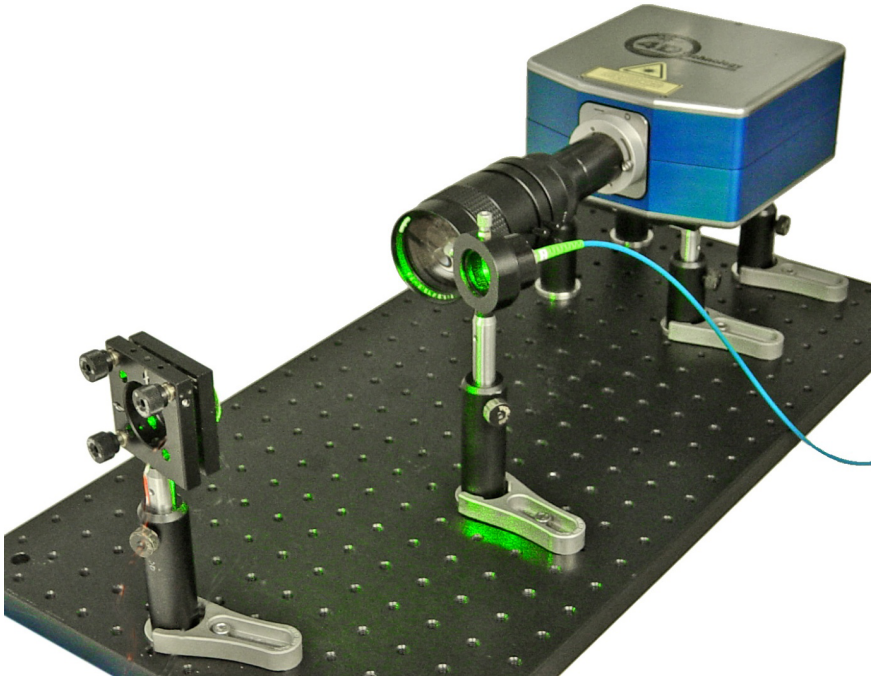

Figure 5: ESPI Test Configuration

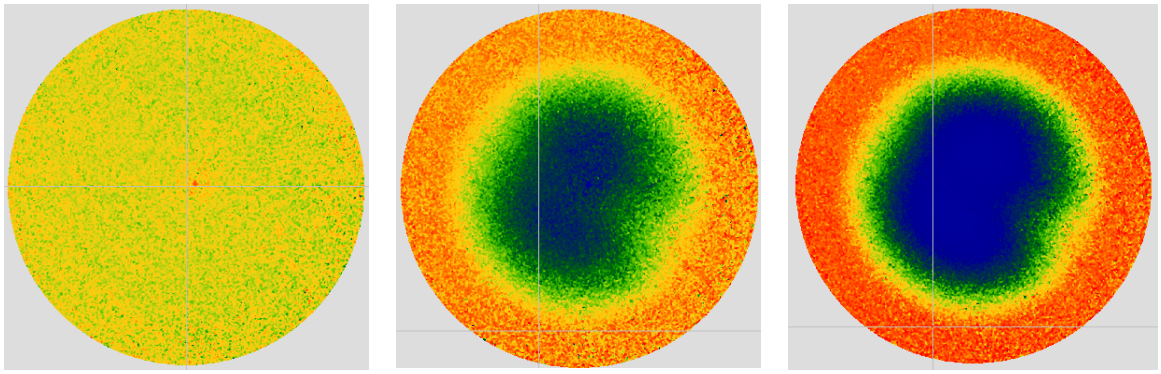

Figure 6: Measurement of Excited Metal Diaphragm

The second dynamic measurement is the change in the wavefront produced by an air burst out of a nozzle. Like the previous measurement the field of view was an area with a diameter of approximately 1.25 inches. The peak to valley of the air flow was approximately 1 wave at 532nm. The successive measurements of the same air flow are shown in Figure 7.

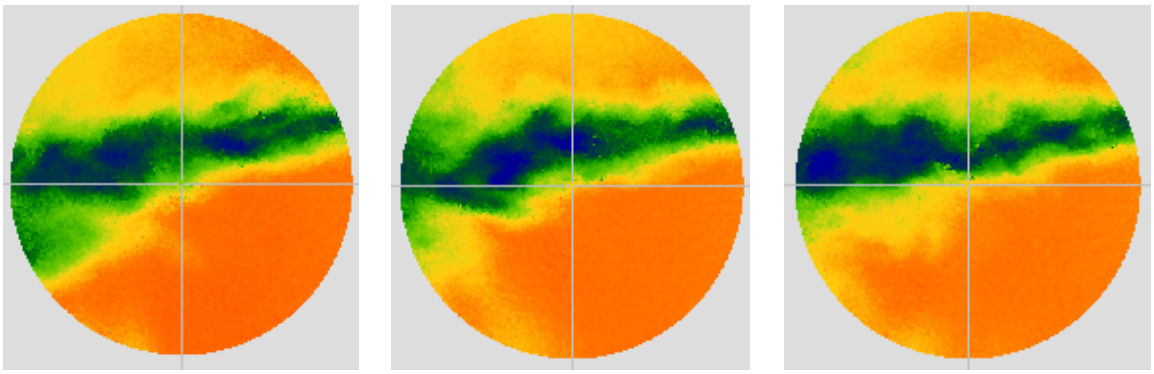

Figure 7: Measurement of air flow emanating from Nozzle.

8. Conclusion

We have demonstrated a flexible dual mode dynamic interferometer capable of measuring both specular and diffuse surfaces with minimal changes between configurations. The interferometer uses a single frame spatial phase-shifting technique that enables camera limited acquisitions times as low as 30μs. The effective integration time can be reduced further by using a pulsed laser or fast switching. As a result the interferometer is able to make quality of dynamic components in noisy environments. As examples a vibrating metal diaphragm and a bust of air were measured in the more challenging ESPI configuration.

---

[1] Millerd, J., et. al., "Pixelated Phase-Mask Dynamic Interferometer," Proc. SPIE 5531, 304-314 (2004)

[2] Kothiyal, P. and Delisle, R., "Shearing interferometer for phase shifting interferometry with polarization phase shifter," Applied Optics 24(24), 4439-4442 (1985)

[3] Greivenkamp, J.E. and Bruning, J.H., PSI Algorithms, in Optical Shop Testing, 2nd Ed., editor D. Malacara, John Wiley and Sons (1992)

[4] Dainty, J.C., "Topics in applied physics volume 9", Springer Verlag, Berlin, (1984).

[5] Nakadate, S., Yatagai, T., and H. Saito, "Electronic speckle pattern interferometry using digital image processing techniques," Applied Optics 19(11), 1879-1883 (1980)

[6] Creath, K., "Phase-shifting speckle interferometry," Applied Optics 24(18), 3053-3058 (1985)

[7] Stetson, K.A., "Optical Sensing and Measurement", Proc. SPIE 1375, 78 (1989)